Cytometry
PART A
Journal of the International Society for Advancement of Cytometry

Fully Automated Analysis of Chemically Induced γH2AX Foci in Human Peripheral Blood Mononuclear Cells by Indirect Immunofluorescence

Annika Willitzki,[1] Sebastian Lorenz,[2] Rico Hiemann,[3] Karina Guttek,[1] Alexander Goihl,[1] Roland Hartig,[1] Karsten Conrad,[4] Eugen Feist,[5] Ulrich Sack,[6] Peter Schierack,[3] Lisa Heiserich,[2] Caroline Eberle,[2] Vanessa Peters,[2] Dirk Roggenbuck,[2,3]*† Dirk Reinhold[1]†

[1]Institute of Molecular and Clinical Immunology, Otto-von-Guericke-University, Magdeburg, Germany
[2]Medipan GmbH, Dahlewitz/Berlin, Germany
[3]Faculty of Sciences, Brandenburg Technical University Cottbus-Senftenberg, Senftenberg, Germany
[4]Institute of Immunology, Technical University Dresden, Dresden, Germany
[5]Department of Rheumatology and Clinical Immunology, Charité-Universitätsmedizin, Berlin, Germany
[6]Institute of Clinical Immunology, Medical Faculty, University of Leipzig, Germany

Received 26 May 2013; Accepted 26 July 2013

*Correspondence to: Prof. Dr. Dirk Roggenbuck, Faculty of Science, Brandenburg Technical University Cottbus-Senftenberg, Großenhainer Str. 57, 01968 Senftenberg, Germany.
E-mail: dirk.roggenbuck@hs-lausitz.de

Published online in Wiley Online Library (wileyonlinelibrary.com)

DOI: 10.1002/cyto.a.22350

†Shared senior authorship.

This work was supported by InnoProfile IP 03 IP 611 funded by the Bundesministerium für Bildung und Forschung (BMBF, Germany).
Conflict of interest: Dirk Roggenbuck is a shareholder of GA Generic Assays GmbH and Medipan GmbH. Both companies are diagnostic manufacturers.

Abstract

Analysis of phosphorylated histone protein H2AX (γH2AX) foci is currently the most sensitive method to detect DNA double-strand breaks (DSB). This protein modification has the potential to become an individual biomarker of cellular stress, especially in the diagnosis and monitoring of neoplastic diseases. To make γH2AX foci analysis available as a routine screening method, different software approaches for automated immunofluorescence pattern evaluation have recently been developed. In this study, we used novel pattern recognition algorithms on the AKLIDES® platform to automatically analyze immunofluorescence images of γH2AX foci and compared the results with visual assessments. Dose- and time-dependent γH2AX foci formation was investigated in human peripheral blood mononuclear cells (PBMCs) treated with the chemotherapeutic drug etoposide (ETP). Moreover, the AKLIDES system was used to analyze the impact of different immunomodulatory reagents on γH2AX foci formation in PBMCs. Apart from γH2AX foci counting the use of novel pattern recognition algorithms allowed the measurement of their fluorescence intensity and size, as well as the analysis of overlapping γH2AX foci. The comparison of automated and manual foci quantification showed overall a good correlation. After ETP exposure, a clear dose-dependent increase of γH2AX foci formation was evident using the AKLIDES as well as Western blot analysis. Kinetic experiments on PBMCs incubated with 5 μM ETP demonstrated a peak in γH2AX foci formation after 4 to 8 h, while a removal of ETP resulted in a strong reduction of γH2AX foci after 1 to 4 h. In summary, this study demonstrated that the AKLIDES system can be used as an efficient automatic screening tool for γH2AX foci analysis by providing new evaluation features and facilitating the identification of drugs which induce or modulate DNA damage.

Key terms

γH2AX foci; automated microscopy; image analysis; DNA double-strand breaks; etoposide; human PBMCs

THE damage of DNA is a critical event able to affect cellular functions and development. Thus, it is essential for cells to maintain DNA integrity and repair such lesions effectively. Among different kinds of DNA lesion, double strand breaks (DSB) are considered to be the most critical type of DNA damage and misrepair can lead to tumorgenesis or cell death (1,2). To ensure detection and repair of DNA damage sites a variety of proteins are involved in different DNA damage response (DDR) pathways (3). After induction of DSB, the histone protein H2AX is rapidly phosphorylated at serine 139, termed γH2AX. Large amounts of γH2AX molecules form a focus in the

chromatin surrounding the DSB site, which is assumed to trigger the accumulation of proteins responsible for DNA damage repair and chromatin remodelling (4,5). Immunofluorescence staining with an anti-γH2AX antibody enables the visualization of these nuclear foci that have been found to correlate with the number of DSB (6,7).

Apart from basic research, analysis of DNA DSB by γH2AX foci detection also has the potential to be used in clinical diagnostics as a biodosimetric tool to examine the effects of high- and low-dose exposure to ionizing radiation and in drug development for drug responsiveness assessments (8–10). To measure the level of γH2AX, different immunologic methods utilizing an anti-γH2AX antibody can be applied. Enzyme immunoassay or immunoblotting techniques allow the determination of the overall γH2AX level in cell or tissue extracts, whereas single cells can be evaluated using flow cytometry applications or microscopy (8). The microscopic immunofluorescence test (IFT) is claimed to be the most sensitive method, enabling the detection of down to only one γH2AX focus per cell as well as colocalization studies with different DDR proteins (5,11,12).

However, visual scoring of γH2AX foci in individual cell nuclei is extremely time consuming and subjective (13,14). Thus, different technical approaches for automated foci quantification have recently been developed to establish fast and standardized γH2AX analysis (14–26). In fact, the majority of currently available applications are based on pure image analysis of previously acquired microscopic images. Depending on the program, the measurement can either be executed in a semi-automatic way, where a user has to investigate the images one by one, or automatically, where a set of images is loaded into the software which further classifies nuclei and foci (13,27). An intriguing development is the RABiT workstation, a fully automated system, which includes every step from cell isolation to γH2AX analysis (28–30). Another system for γH2AX foci evaluation, combining automated image acquisition, image processing, and image analysis is the AKLIDES® platform.

In our study, we used the AKLIDES system to analyze drug-induced γH2AX foci formation in human peripheral blood mononuclear cells (PBMCs). First, we compared the γH2AX level obtained through automated image analysis with data achieved by manual scoring and immunoblotting of etoposide (ETP)-treated PBMCs. Then, the AKLIDES system was used to study foci formation kinetics and recovery behavior. Furthermore, PBMCs were treated with different immunosuppressive agents to investigate whether these substances are capable of inducing γH2AX foci formation.

The results that will be discussed show that the AKLIDES system can be a helpful tool for automated γH2AX screening.

Materials and Methods

Separation and Cell Culture of Human PBMCs

PBMCs were obtained from heparinized blood of healthy volunteer donors and isolated by density gradient centrifugation using Biocoll separating solution (Biochrom, Berlin, Germany). A vote of the local ethical committee for using human blood was obtained. After separation, PBMCs were washed and resuspended to a final density of 1 x 10^6 cells/ml in RPMI 1640 (Biochrom) containing 10% fetal bovine serum (Pan Biotech, Aidenbach, Germany) 100 U/ml penicillin and 100 µg/ml streptomycin (both Life Technologies GmbH, Darmstadt, Germany). For treatment, 500 µl per sample of cell suspension were seeded into 48-well plates, or 1 ml into 24-well plates respectively, and incubated at 37°C with 7% CO_2. To analyze the effect of different drugs in γH2AX foci formation, cells were stimulated overnight either with etoposide (ETP; Sigma, St. Louis, USA), camptothecin (CPT; Abcam, Cambridge, UK), daunorubicin (DNR; Sigma), cytarabine (AraC; Sigma), cyclosporine A (CsA; Sigma), dexamethasone (Dexa; Sigma), rapamycin (Rapa; Sigma), active TGF-β1 (R&D Systems, Minneapolis, USA) or anti-TNF-α antibody (Golimumab; MSD Sharp & Dohme, Haar, Germany), which were added into the plates at the indicated concentrations.

For kinetic and recovery analysis, PBMCs were treated directly with ETP. After 1 h, one part of the cells was centrifuged and resuspended into fresh medium. Subsequently, PBMCs were dispensed into 24-well plates and incubated at 37°C and 7% CO_2. Afterwards, the cells were harvested and fixed at the indicated time points.

Immunofluorescence Staining

Cell fixation and staining was performed using a γH2AX immunofluorescence staining kit (Medipan, Berlin/Dahlewitz, Germany). The γH2AX assay was carried out according to the manufacturer's instructions with modifications regarding cell seeding. Briefly, cells were transferred from a 48-well culture plate into 1.5 ml tubes and centrifuged for 12 min at 200*g*. Supernatants were discarded and PBMCs resuspended in cold PBS to a density of 1.5 x 10^6 cells/ml. Subsequently, the cells were pipetted onto silanized glass slides at about 4 x 10^4 cells per spot and fixed for 15 min in 4% formaldehyde. Slides were washed three times for 10 min each in PBS. Permeabilization was performed for 5 min at 4°C with 0.1% Triton in PBS containing 1% BSA. After washing the slides three times for 10 min each in PBS with 1% BSA, 25 µl anti-phosphohistone H2AX mouse monoclonal IgG antibody (1:200; Millipore, Schwalbach, Germany) were added and incubated for 1 h at room temperature. Afterwards cells were washed again three times in PBS with 1% BSA for 10 min each and incubated with 25 µl goat anti-mouse IgG conjugated to Alexa Fluor 488 (1:500; Invitrogen, Darmstadt, Germany) for 1 h in the dark. After a final washing cycle in PBS, cells were covered with 4′,6-diamidino-2-phenylindole (DAPI) containing mounting solution (Medipan, Berlin/Dahlewitz, Germany).

Western Blotting

Measurement of γH2AX level by Western blotting analysis was performed using a modified protocol based on the publication by Redon et al. (5). In brief, after drug treatment 1 x 10^6 PBMCs were transferred from a 24-well plate into 1.5 ml tubes and centrifuged at 2,000*g* for 5 min. Supernatants were discarded and cells were washed in 800 µl ice cold PBS containing 10 mM NaF. After centrifugation at 2,000*g* for 5 min at 4°C supernatants were removed and cell pellets were resuspended in 60 µl hot 1x reducing SDS sample buffer. Cells

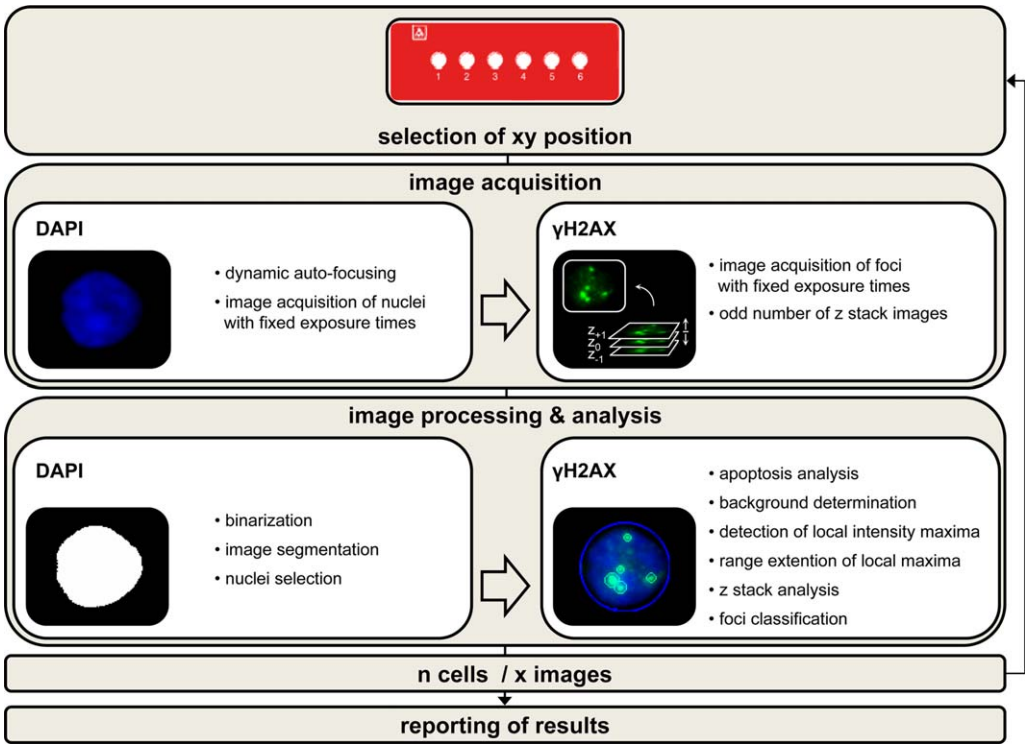

Figure 1. Flow chart of main processes involved in automated γH2AX foci quantification. After insertion of slides into the system and starting of the measurement, corresponding *xy*-positions of the wells were accessed. Using dynamic auto-focusing, the exact focal plane was automatically detected in DAPI channel and an image of the nuclei was acquired. Subsequently, the light source switched to 488 nm to illuminate γH2AX foci and an image at the determined *z*-plane as well as one image 1 μm above and 1 μm below this plane was recorded. DAPI images were further automatically processed to evaluate cell nuclei. For each nucleus, the corresponding three images in the γH2AX foci channel were analyzed to exclude apoptotic cells and to identify the number of γH2AX foci per cell. Different *xy*-positions per well were analyzed until at least 100 cells were detected. Subsequently, the next well was evaluated. After the measurement, results were reported as Excel- and PDF-files. [Color figure can be viewed in the online issue, which is available at wileyonlinelibrary.com.]

were boiled for 10 min at 95°C, subsequently chilled on ice and centrifuged for 5 min at 16,000*g* at 4°C. Supernatants were collected and stored at −20°C until further use. For SDS polyacrylamide gel electrophoresis (SDS-PAGE), 20 μl of each lysate were loaded onto the lanes of a 12.5% SDS gel. After blotting the gel onto nitrocellulose, the membrane was blocked with 5% milk powder (Roth, Karlsruhe, Germany) in 1 x Tris buffered saline solution (TBS) for 1 h. The membrane was incubated overnight with anti-γH2AX antibody (Millipore) diluted 1:2000 in TBS containing 3% BSA. After washing, the membrane was incubated for 1 h with 1:10,000 diluted donkey-anti-mouse HRP-conjugated secondary antibody (Dianova, Hamburg, Germany), washed again and finally binding was detected using ECL substrate (ThermoScientific, Rockford, USA). The intensity of individual Western blot bands was determined with Kodak Image Station quantification software. Each quantified value of anti-γH2AX was normalized to the corresponding intensity of the β-actin loading control. Results were displayed as relative γH2AX levels in relation to the value of untreated PBMCs.

Manual Foci Analysis

Manual γH2AX foci quantification was performed on DAPI- and γH2AX-merged images acquired by the AKLIDES system. For each sample, an average number of 6 images was analyzed covering altogether between 105 and 146 selected nuclei. Cell morphology was judged on the basis of the DAPI staining, and strongly damaged nuclei and apoptotic cells as well as granulocytes were excluded from the evaluation.

Automated γH2AX Foci Analysis

The AKLIDES system (Medipan, Berlin/Dahlewitz, Germany) was designed and constructed for fully automated evaluation of immunofluorescence patterns in autoantibody detection (31–33). As described in detail elsewhere (22,23,33), it is based on a motorized inverse fluorescence microscope (Olympus IX81, Olympus, Hamburg, Germany) controlled by innovative software providing fully automated image acquisition, analysis, and evaluation of IFT. For automated fluorescence image acquisition, the microscope includes an objective with 60 x magnification (Olympus, semi-apochromat LUCPLFLN 60X, 0.70 NA, W.D.1.5 – 2.2 mm), a multiband filter for the DAPI and Alexa 488 dyes (DA/FI-A, Semrock, Lake Forest, USA), 400 nm and 490 nm light emitting diodes (pE-2, CoolLED, Andover, UK) and a charge-coupled device (CCD) gray level camera (DX4, Kappa optronics, Gleichen, Germany).

Automated γH2AX analysis by the AKLIDES system comprises a sequential process including image acquisition and multiple steps used for object identification and classification (Fig. 1). First slides are inserted into the motorized stage, and

the respective wells are selected by their defined xy positions. Two different fluorescent dyes are required for automated γH2AX foci analysis. Thus, DAPI counterstaining is used for autofocusing, nuclei identification and morphological characterisation of nuclei (22,23,33). Applying Alexa488-conjugated secondary antibody, γH2AX foci are separately analyzed in the green foci channel.

Autofocusing based on Haralick's characterization of image texture is used to find the exact focal plane of the nuclei in the DAPI channel. Employing a 60x magnification and defined exposure times after focussing, one two-dimensional DAPI image is acquired. Furthermore, a three image z-stack in the foci channel with 1 μm distance is obtained, including an additional image of γH2AX foci in a layer 1 μm above and 1 μm below the primary focal plane. Images are stored lossless as tagged image files (TIF) and analyzed using different software algorithms. To identify cell nuclei in the DAPI images, histogram-based binarization using background describing modus for global thresholding is performed. Objects are segmented with a watershed algorithm and afterwards filtered according to previously known nucleus size. In order to exclude monocytes, granulocytes, cell aggregates, and heavily damaged cells among the identified objects, morphological parameters are applied for nuclei selection (ratio of maximum and minimum radius, convexity). The nucleus of selected cells have to have a diameter between 4 and 10 μm and, in order to incorporate the shape and roundness of the cell, only nuclei with a convexity between 0.9 and 1.0 and a ratio <1.3 are selected. Apoptosis induces a pan-nuclear γH2AX phosphorylation. Therefore, selected cells are scored as apoptotic, when more than 70% of the nucleus area detected in DAPI mode also exceeds the threshold in the foci channel. For non-apoptotic cells, the background intensity in every *z*-plane for each selected nucleus and local intensity maxima in the merged *z*-plane image is determined. A region growing algorithm is used to extend the range of the local maxima in order to identify the focus area. Binarization and image segmentation is performed separately in every *z*-plane of all identified focus areas. Subsequently, objects are classified as foci when the determined size and intensity reaches the defined threshold which is specific for each cell line. The range of a focus diameter is set between 0.25 and 1.2 μm. Foci bigger than 1.2 μm are assigned as clusters. Further cluster analysis is performed by determining the cluster size and the suitable number of foci which fit into this area. For each sample a minimum of hundred cells are analyzed and different parameters, such as number of selected cells, average foci number/cell, mean intensity, and number of γH2AX-positive cells are calculated. After the measurement is finished, an xls-file and a PDF-report displaying these different parameters for all analyzed samples is generated.

RESULTS

Comparison of Manual, Automated, and Immunoblot Analysis of ETP-Induced γH2AX Formation

To evaluate automated γH2AX foci quantification by the AKLIDES system, PBMCs were treated overnight with different concentrations of ETP, a cytostatic drug known to induce DNA DSB (34). Afterwards cells were fixed on slides and stained for phosphorylated histone H2AX. As expected, treatment of PBMCs with ETP led to an increase in γH2AX foci formation in a dose dependent manner, which is illustrated in images taken by the AKLIDES system shown in Figure 2A. Next, slides with PBMCs treated with different concentrations of ETP were analyzed by the AKLIDES system and images were also scored manually. Consequently, 100–150 nuclei per sample obtained from four different donors and dilution series were analyzed, with granulocytes, cell aggregates as well as highly damaged or apoptotic cells excluded from the measurement. Comparison of the results from manual and automated scoring of microscope images revealed a good agreement of both methods (Pearson correlation coefficient $r = 0.9827$, $P < 0.0001$) (Fig. 2B).

A dose-dependent increase of γH2AX levels after ETP treatment of PBMCs was also confirmed using Western blot analysis (Fig. 2C). It has to be noted that in this method all cells of the sample were lysed, and in particular apoptotic or damaged cells could not be excluded from the analysis.

To compare γH2AX foci quantification and Western blot analysis, the relative γH2AX level of the mean values were calculated according to the corresponding untreated control. As shown in Figure 2D, both methods revealed a linear dose response behavior but show a significant difference in the slope of their linear fit (coefficients after linear regression: AKLIDES scoring with additional cluster analysis: $R^2 = 0.998$, slope = 6.14 ± 0.15, $P < 0.0001$; Western blot: $R^2 = 0.995$, slope = 0.58 ± 0.02, $P < 0.0001$), (Student's *t*-test of the slopes: $P < 0.0001$).

Comparison of Different Parameters by Automated γH2AX Analysis

Unlike visual scoring or Western blot analysis, where either foci numbers or total γH2AX levels are determined respectively, automated measurement using the AKLIDES® system enables users to evaluate a variety of different parameters. To investigate which of these parameters are useful to study the formation of γH2AX foci, respective foci number with and without additional cluster evaluation, cell intensity as well as the percentage of γH2AX-positive PBMCs after treatment with ETP for 16 h were determined (Figs. 3A–3D). Additionally, formation of γH2AX foci clusters according to the applied ETP concentration was investigated (Figs. 3E,3F).

For ETP concentrations up to 10 μM the average number of γH2AX foci per cell was found to be similar, irrespective of additional cluster evaluation. A significant difference between the foci number with and without cluster evaluation was calculated for PBMCs treated with 20 μM ETP (paired Student's *t*-test, $P < 0.0001$). The dose response curve of the mean values after cluster evaluation remains linear (coefficient of determination: linear fit of data points 0 – 10 μM ETP $R^2 = 0.999$; linear fit of data points 0 μM – 20 μM ETP: $R^2 = 0.997$), whereas without additional evaluation the dose response curve loses linearity as ETP concentration increases (coefficient of determination: linear fit of data points 0 μM–10 μM ETP: $R^2 = 0.995$; linear fit of data points 0 μM – 20

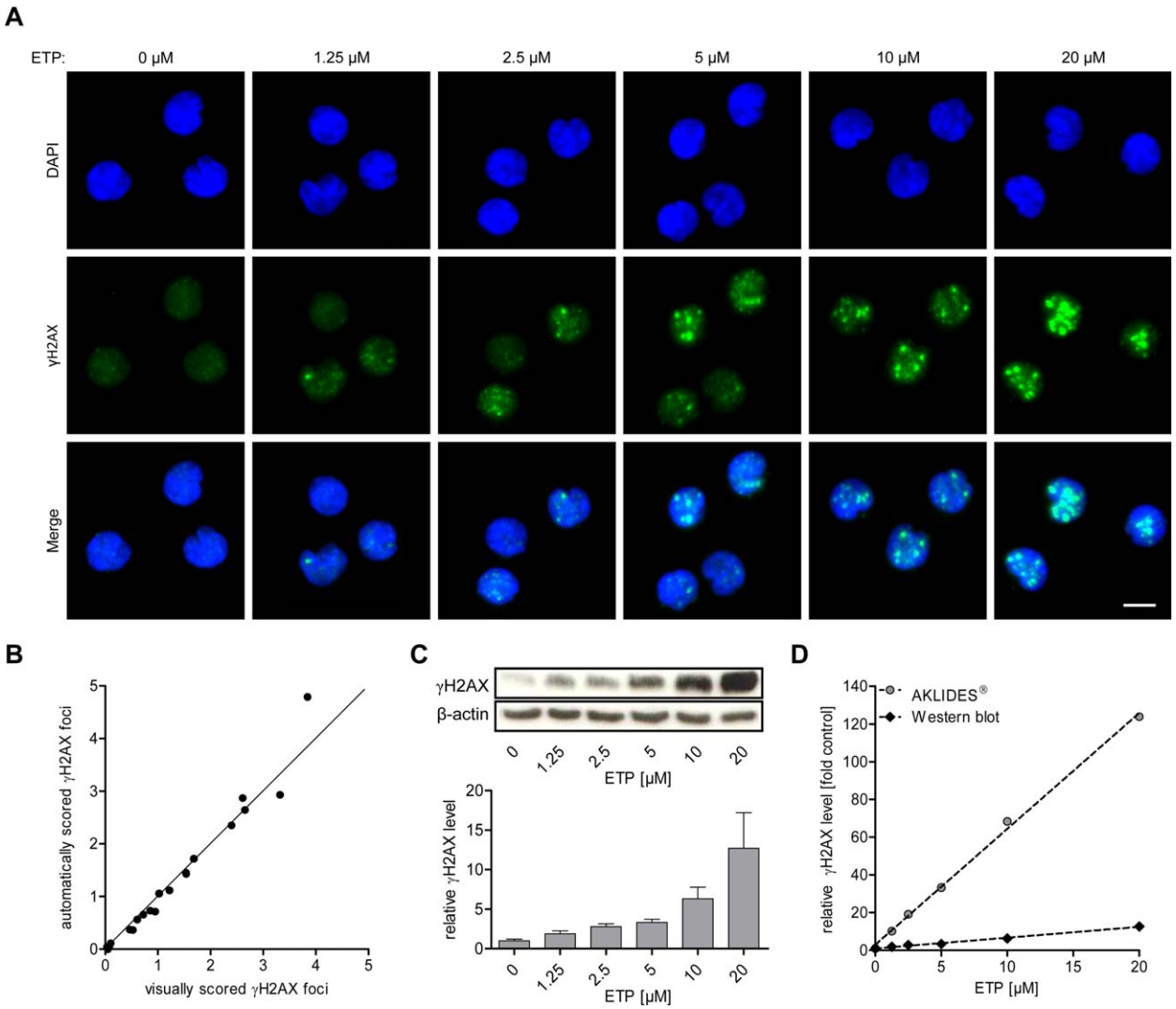

Figure 2. Dose-dependent increase of γH2AX formation after treatment of PBMCs with differing concentrations of etoposide (ETP) for 16 h. **A**: Images taken by the AKLIDES® system after γH2AX (green) immunofluorescence staining and DAPI counterstaining (blue) of ETP-treated PBMCs fixed on slides (scale bar 5 μm). **B**: Each data point represents the average focus number per nucleus of ETP-treated PBMCs determined visually as well as by automated foci quantification (without additional cluster evaluation). In general, 100–150 cells of $n = 20$ samples were analyzed. A line through the origin with slope = 1 was drawn for comparison. **C**: Relative γH2AX levels in PBMC lysates analyzed with SDS-PAGE followed by Western blotting. The upper panel illustrates representative images of immunoblot staining against γH2AX and the corresponding β-actin control. The lower diagram shows the quantification of γH2AX levels normalized to the corresponding β-actin controls, reported as folds of γH2AX levels in untreated PBMCs. Each bar represents the mean + SEM of $n = 4$ independent experiments. **D**: Comparison of the dose dependent increase in γH2AX levels normalized to the respective control by automated γH2AX foci scoring (with additional cluster evaluation) and γH2AX level quantification by Western blot analysis. Data points show the mean of $n = 4$ independent experiments. [Color figure can be viewed in the online issue, which is available at wileyonlinelibrary.com.]

μM ETP: $R^2 = 0.964$) (Fig. 3A). Linear response behavior can also be observed among the mean values of cell intensity (coefficient of determination: $R^2 = 0.997$) (Fig. 3B). Depending on the donor, an average of 4.27 $\pm$ 3.59% of untreated PBMCs were found to be γH2AX-positive, and with increasing ETP concentration the curve representing the ratio of γH2AX-positive and γH2AX-negative cells started to reach a plateau (Fig. 3C). Furthermore, a correlation between foci number and intensity signal of ETP-treated PBMCs (Spearman $r = 0.9731$) can be shown (Fig. 3D).

Clustering of γH2AX foci was observed, showing a linear increase in the number of γH2AX clusters formed per cell with rising ETP concentrations (Fig. 3E). To further analyze the impact of cluster analysis on the determined foci number, the ratio between separate foci and foci accumulated in clusters was calculated. The analysis showed an increase in fused foci with elevation of ETP concentration, leading with 20 μM ETP to a ratio of 54 $\pm$ 10% of foci existing as separate entities, whereas 46 $\pm$ 10% of detected foci were merged in clusters (Fig. 3F).

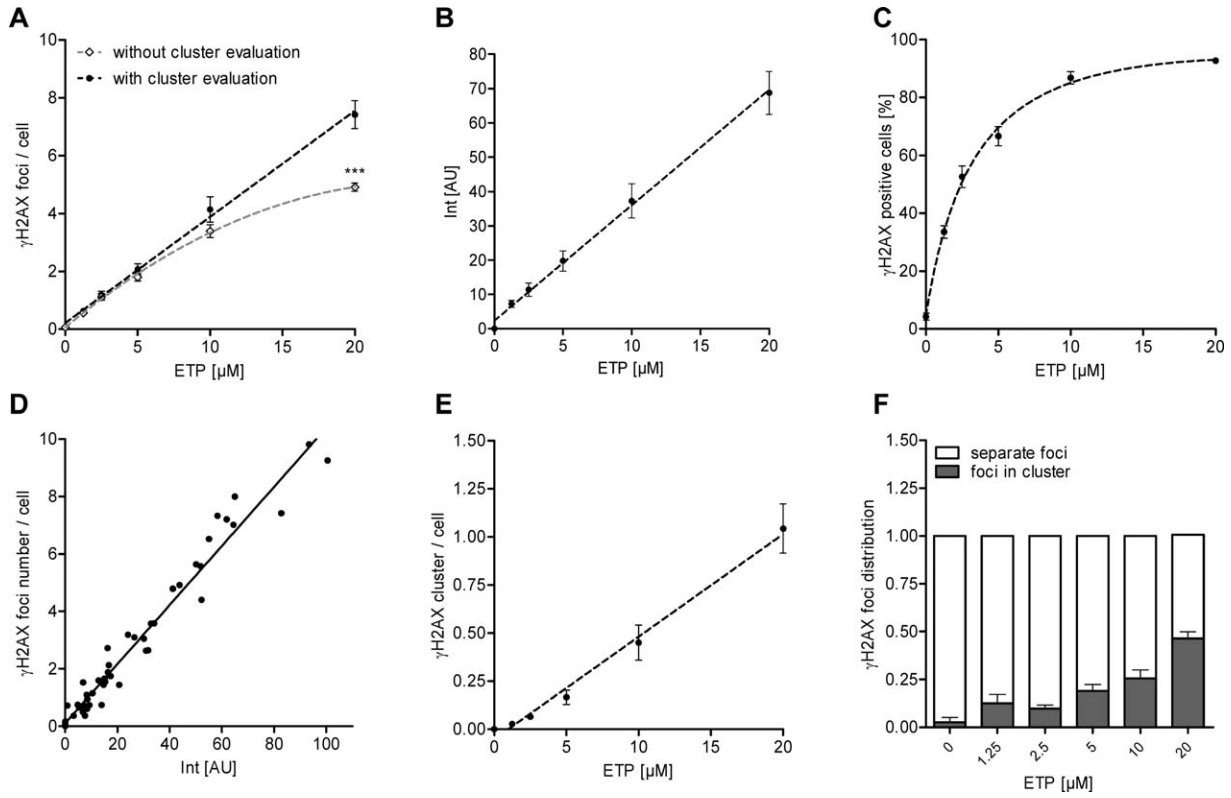

Figure 3. Automatic γH2AX foci analysis of PBMCs treated with rising concentrations of ETP for 16 h. **A**: Linear dose response in γH2AX foci number after cluster analysis (filled circles) and saturation behavior of the dose response curve without further cluster analysis (open diamonds). **B**: Linear dose response in γH2AX fluorescence intensity (Int, displaying intensity signal minus corresponding background signal of untreated cells) of ETP treated PBMCs. **C**: Ratio of γH2AX foci-positive and γH2AX foci-negative cells after treatment with different concentrations of ETP. **D**: Correlation between γH2AX foci number per cell after additional cluster analysis and average nuclear fluorescence intensity (intensity signal minus corresponding background signal of untreated cells). **E**: Linear dose response behavior in γH2AX cluster formation. **F**: Ratio between the number of separate γH2AX foci and foci accumulated in clusters. Data points represented as mean ± SEM of $n = 9$ experiments.

Kinetics of γH2AX Foci Formation and Recovery Behavior of PBMCs Upon ETP Treatment

The formation of γH2AX foci is reported to be one of the fastest events after induction of DNA DSB. In the next test setting, the AKLIDES system was used to analyze γH2AX foci formation kinetics in ETP-treated PBMCs. Cells were incubated with 5 μM ETP, harvested, and fixed 0.5 h to 24 h after the beginning of treatment. ETP was not removed during the whole incubation time. In a second experimental setup PBMCs were treated with 5 μM ETP for 1 h. Afterwards the cells were washed, resuspended in fresh ETP-free medium and also harvested and fixed at indicated time points. Anti-γH2AX immunofluorescence staining was performed and slides were analyzed using the automated evaluation by the AKLIDES system. Under the employed conditions, maximal foci numbers were reached after 4–8 h of ETP treatment (Fig. 4A). Furthermore, a maximum was also observed after 4–8 h in the relative amount of γH2AX-positive cells (Fig. 4B). Samples analyzed 12 h and 24 h after the beginning of treatment revealed a decrease in γH2AX numbers, as well as a reduction in γH2AX positive cells, even though the ETP was not removed. The kinetics of PBMCs being exposed to ETP for only 1 h demonstrated an increase in γH2AX numbers and in the amount of γH2AX-positive cells 30 min after ETP removal (Figs. 4A and 4B). After 1 h of recovery time, a γH2AX level comparable with the initial value was reached, followed by a strong decrease of 72% measured 3 h after ETP removal, regarding the average γH2AX number/cell as well as the amount of γH2AX-positive cells. No significant differences in the number of γH2AX per cell as well as in the percentage of γH2AX-positive cells was observed between untreated PBMCs and PBMCs treated for 1 h with ETP 24 h post exposure (Figs. 4A and 4B).

Effects of Immunosuppressive Agents on γH2AX Foci Formation

Different studies have shown that cytostatics like ETP are capable of inducing γH2AX foci in human PBMCs (34). Since there is also evidence that immunosuppressive drugs like CsA or Rapa influence DNA repair, we wanted to investigate the effects of different classes of immunosuppressives on PBMCs with respect to γH2AX foci formation (35–37). Therefore, PBMCs were treated overnight with different immunosuppressive agents, either CsA (10 μM), Rapa (10 μM), Dexa (10 μM), ETP (10 μM), CPT (2.5 μM), DNR (50 nM), AraC (2.5 μM), active TGF-β1 (10 ng/ml) or anti-TNF-α (100 μg/ml). Concentrations of CsA, Rapa, Dexa and TGF-β1 were used

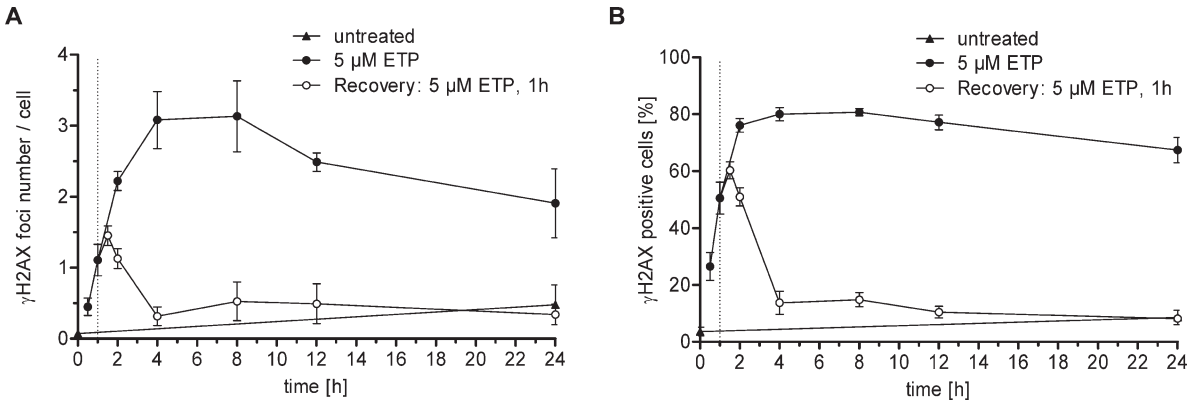

Figure 4. Kinetics of γH2AX foci formation during continuous treatment of PBMCs with ETP (black circles) as well as recovery behavior after removal of ETP present for 1 h (white circles). Untreated PBMCs are represented by gray triangles. Cells were harvested and fixed at different time points between 0 and 24 h of treatment. Immunofluorescence staining against γH2AX was performed and slides were analyzed automatically by the AKLIDES® system. **A**: Kinetics of γH2AX foci formation and (**B**) percentage of γH2AX focus-positive cells analyzed at different time points. Data represent mean ± SEM of $n = 4$ independent experiments.

according to proliferation assays in a range where significant suppression of DNA synthesis was observed (data not shown). The concentrations of the cytostatic reagents ETP, CPT, DNR, and AraC were further reduced to an amount where the induced level of γH2AX foci were similar, and did not exceed the maximal value that can be analyzed either in γH2AX foci measurement using the AKLIDES system or in Western blot quantification.

Analysis of γH2AX foci formation after treatment of PBMCs with these immunosuppressants showed that only the cytostatic reagents ETP, CPT, DNR, and AraC induced DSB (Fig. 5A). Treatment with different drugs known to suppress the immune response did not result in a significant rise in γH2AX foci formation (1way ANOVA, $P < 0.001$). Slightly different results revealed the measurement of γH2AX levels in cell lysates using Western blot analysis (Fig. 5B). Although a significant rise in γH2AX levels was also observed after treatment with ETP, CPT, DNR, and AraC (1-way ANOVA, $P < 0.05$) the folds of increase differed from IFT results. Furthermore, elevated γH2AX levels were detected in PBMCs treated with Rapa and Dexa in Western blot analysis.

DISCUSSION

Since the phosphorylation at serine 139 of H2AX was first described in 1998 as a consequence of DNA DSB, the field of γH2AX applications has been constantly growing (4,38). Being identified as a biomarker for aging and cancer, many studies have been performed utilizing γH2AX foci formation as an individual biodosimeter for cell or body radiation exposure, for drug treatment and development as well as a parameter to study a potential genotoxic impact caused by different environmental agents (9).

The most common method currently used to analyze γH2AX foci formation is the visual scoring of immunofluorescence stained γH2AX foci, either directly with a fluorescent microscope, or by examining microscopic images which were previously taken (5,11,12). However, visual evaluation is time consuming, prone to subjectivity, and is therefore unsuitable for high-throughput screening (15). Furthermore, it lacks standardization and is characterized by high intra- and interlaboratory scoring variability (22). To overcome limitations of manually analyzed γH2AX assays, a variety of software solutions were developed enabling automated foci quantification. Most of these methods are based on image analysis of previously acquired (confocal) microscopic images (14–26). In contrast to pure image processing, the automated γH2AX evaluation by the AKLIDES system combines image acquisition, processing, and analysis.

Hiemann et al. previously reported the development of the automated AKLIDES® system to improve the evaluation and standardization of cell-based immunofluorescence tests for autoantibody detection (23,32,33). The platform was subsequently further developed to allow automated detection of DAPI counterstained nuclei and γH2AX foci pattern analysis. Results of automated γH2AX foci measurements in irradiated PC Cl3 cells using the AKLIDES system were previously published by Runge et al. (22). In this study, the software was optimized to analyze human PBMCs and novel algorithms were developed, allowing in particular the evaluation of overlapping foci.

Results achieved through automated γH2AX assessment were compared with visually analyzed images. This analysis revealed a high agreement between visual and automated scoring, proving the AKLIDES technology to be a reliable tool for γH2AX evaluation. The comparison of γH2AX assessment by immunofluorescence staining with data achieved by Western blot analysis demonstrated a difference in assay sensitivity between these two methods. According to Berson and Yalow, assay sensitivity can be measured by the slope of the dose-response curve (39). Displaying the ETP concentration on the *x*-axis and the fold of increase in γH2AX level relative to the control on the *y*-axis, the slope of automated foci quantification was more than 10 times higher than the slope of the dose-response curve referring to Western blot determination. This confirmed the lower sensitivity of Western blot analysis described previously (34).

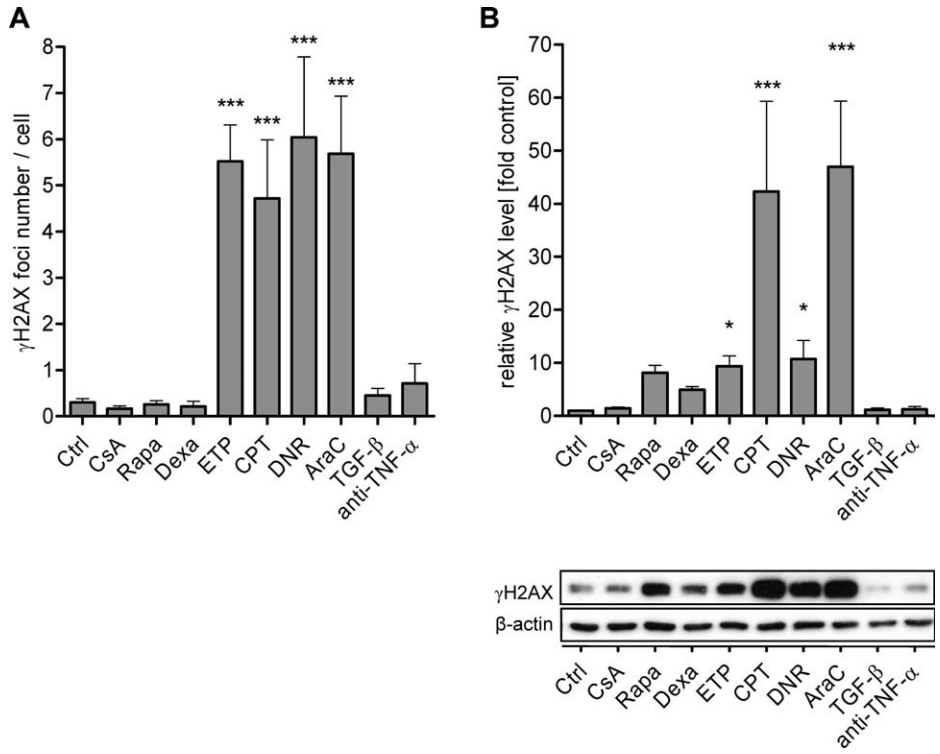

Figure 5. Induction of γH2AX formation in PBMCs after treatment with different immunosuppressive reagents. PBMCs were treated over night with either 10 μM cyclosporine A (CsA), 10 μM rapamycin (Rapa), 10 μM dexamethasone (Dexa), 10 μM etoposide (ETP), 2.5 μM camptothecin (CPT), 50 nM daunorubicin (DNR), 2.5 μM cytarabine (AraC), 10 ng/ml active TGF-β1 or 100 μg/ml anti-TNF-α antibody. **A**: γH2AX foci quantification performed by the automated AKLIDES® system of immunofluorescence stained PBMCs. Each bar represents the mean + SEM of at least $n = 4$ independent experiments. **B**: Relative γH2AX levels in PBMC lysates were determined by Western blot analysis. The upper diagram shows the quantification of γH2AX levels normalized to β-actin controls, referring to the folds of untreated PBMCs. Each bar represents the mean + SEM of at least $n = 4$ independent experiments. The lower panel illustrates representative images of immunoblot staining against γH2AX and the corresponding β-actin control.

Apart from simple γH2AX foci quantification, automated measurement by the AKLIDES system enables the analysis of additional parameters such as focus size, focus and overall nuclear intensity, co-localization with differently stained molecules as well as the application of correction or evaluation algorithms. The observed linearity of the dose-response relationship with the number of γH2AX foci scored was shown to be limited with higher ETP levels, whereas it was sustained when related to the measurements of the intensity of γH2AX foci per cell. This phenomenon is mainly due to γH2AX clustering, which results from focus merging when the number of foci per nucleus increases (18).

To address the issue of underestimated focus assessment, an additional algorithm was implemented into the software to calculate the actual focus number of these clusters. By analyzing the cluster area and dividing it by the average size of a single focus, the number of foci accumulated in a cluster was estimated. After applying this additional cluster evaluation, linearization of the dose-response curve for γH2AX foci quantification even at high ETP doses of up to 20 μM could be observed. Therefore, additional cluster evaluation was included for measuring the average focus number per cell in subsequent experiments.

Besides dose dependency, we also studied time-dependent formation of γH2AX foci and recovery behavior using ETP treated PBMCs and automated foci quantification. Cells constantly incubated with 5 μM ETP revealed an increase of γH2AX foci even after 30 min and peaked after 4 to 8 h. After 8 to 12 h the number of γH2AX foci started to decrease. This reduction can be due to a diminished ETP concentration, since instability of ETP has been described *in vitro* with different degradation kinetics depending on culture conditions (40). The recovery behavior and γH2AX deletion were studied in PBMCs treated for 1 h with ETP and subsequently suspended in ETP-free medium. Cells fixed 30 min after ETP was washed out still revealed an increase in γH2AX foci numbers, compared to cells already fixed 1 h after ETP treatment. With progressing recovery time γH2AX foci started to decrease, and cells reached a level comparable to untreated cells after 24 h. The same behavior could be seen by evaluating the amount of γH2AX positive cells. Experiments analyzing human peripheral blood lymphocytes exposed to ionizing radiation (IR) also showed a linear dose-response behavior and a decline in γH2AX foci starting 30 min after irradiation (41). The number of γH2AX foci measured 24 h after IR exposure was found to be proportional to the initial radiation dose, and the amount of γH2AX foci

reached a level comparable to untreated cells when the initial foci number was less than 5 foci per cell, similar to the value determined in our study.

In previous publications, it was shown that γH2AX foci are induced upon treatment with various cytostatics used in chemotherapy (26,34). Since it was also described that immunosuppressive drugs such as CsA or Rapa affect DNA damage, we wanted to investigate whether treatment of PBMCs with different classes of immunosuppressive drugs can induce γH2AX foci formation (35–37,42–44). To investigate the effects of several immunomodulatory agents on DNA DSB and γH2AX foci formation, PBMCs were treated overnight with either CsA, Rapa, Dexa, ETP, CPT, DNR, AraC, active TGF-β1 or anti-TNF-α. The γH2AX levels were determined through immunofluorescence staining as well as by Western blot analysis. Performing automated γH2AX foci quantification, we could confirm a significant increase in foci formation after treatment of PBMCs with the cytostatics ETP, CPT, DNR, and AraC. Although previously performed proliferation assays (data not shown) using the same concentrations of CsA, Rapa, Dexa, and active TGF-β1 revealed a reduction in ^{3}H-thymidine uptake of T cells, these agents as well as the immunomodulatory anti-TNF-α- antibody did not show a significant change in γH2AX foci formation investigated with IFT. A slightly different result was obtained with Western blot analysis. A significant increase in γH2AX level was also detected for all four cytostatic agents ETP, CPT, DNR, and AraC, even though their significances differed partially from IFT measurements. Furthermore, Western blot analysis revealed an increase of γH2AX levels in the cell lysate of PBMCs treated with Rapa and Dexa, which could not be observed in microscopy analysis. This effect might be due to an increase of apoptotic cells after Rapa or Dexa treatment. Specific measurement of apoptosis was not performed, but investigation of cell morphology and γH2AX staining of microscopic images taken from comparable samples revealed an increase in apoptotic cells. Notably, pan-nuclear staining of γH2AX can be observed during apoptosis. Therefore apoptotic cells can be excluded from automated foci quantification, whereas their influence cannot be eliminated in Western blot analysis. This might be the reason for the different results obtained by these two detection methods.

In conclusion, the computational approach presented in this study proved to be a fast and reliable tool for automated γH2AX foci analysis. Comparing automated foci quantification of ETP treated PBMCs demonstrates a good correlation with results obtained by visual scoring. Furthermore, the AKLIDES system uses algorithms that allow automated image acquisition, nuclei identification, exclusion of apoptotic cells, and cluster evaluation of overlapping or fused foci. Here we were able to show that the AKLIDES system is a reliable tool to analyze the effects of different reagents on DNA DSB and γH2AX formation.

LITERATURE CITED

1. Khanna KK, Jackson SP. DNA double-strand breaks: Signaling, repair and the cancer connection. Nat Genet 2001;27:247-254.
2. Jackson SP. Sensing and repairing DNA double-strand breaks. Carcinogenesis 2002; 23:687-696.
3. Cline SD, Hanawalt PC. Who's on first in the cellular response to DNA damage? Nat Rev Mol Cell Biol 2003;4:361-372.
4. Rogakou EP, Pilch DR, Orr AH, Ivanova VS, Bonner WM. DNA double-stranded breaks induce histone H2AX phosphorylation on serine 139. J Biol Chem 1998;273: 5858-5868.
5. Redon CE, Nakamura AJ, Sordet O, Dickey JS, Gouliaeva K, Tabb B, Lawrence S, Kinders RJ, Bonner WM, Sedelnikova OA. gamma-H2AX detection in peripheral blood lymphocytes, splenocytes, bone marrow, xenografts, and skin. Methods Mol Biol 2011;682:249-270.
6. Rothkamm K, Lobrich M. Evidence for a lack of DNA double-strand break repair in human cells exposed to very low x-ray doses. Proc Natl Acad Sci USA 2003;100: 5057-5062.
7. Redon CE, Nakamura AJ, Gouliaeva K, Rahman A, Blakely WF, Bonner WM. The use of gamma-H2AX as a biodosimeter for total-body radiation exposure in non-human primates. PLoS One 2010;5:e15544.
8. Redon CE, Nakamura AJ, Zhang YW, Ji JJ, Bonner WM, Kinders RJ, Parchment RE, Doroshow JH, Pommier Y. Histone gammaH2AX and poly(ADP-ribose) as clinical pharmacodynamic biomarkers. Clin Cancer Res 2010;16:4532-4542.
9. Redon CE, Nakamura AJ, Martin OA, Parekh PR, Weyemi US, Bonner WM. Recent developments in the use of gamma-H2AX as a quantitative DNA double-strand break biomarker. Aging (Albany NY) 2011;3:168-174.
10. Redon CE, Weyemi U, Parekh PR, Huang D, Burrell AS, Bonner WM. gamma-H2AX and other histone post-translational modifications in the clinic. Biochim Biophys Acta 2012;1819:743-756.
11. Rothkamm K, Horn S. gamma-H2AX as protein biomarker for radiation exposure. Ann Ist Super Sanita 2009;45:265-271.
12. Muslimovic A, Johansson P, Hammarsten O. Measurement of H2AX phosphorylation as a marker of ionizing radiation induced cell damage. In: Nenoi M, editor. Current Topics in Ionizing Radiation Research. Rijeka: InTech; 2012. pp 3-20.
13. Roch-Lefèvre S, Valente M, Voisin P, arquinero JF. Suitability of the ?-H2AX assay for human radiation biodosimetry. In: Nenoi M, editor. Current Topics in Ionizing Radiation Research. Rijeka: InTech; 2012. pp 21-30.
14. Ivashkevich A, Redon CE, Nakamura AJ, Martin RF, Martin OA. Use of the gamma-H2AX assay to monitor DNA damage and repair in translational cancer research. Cancer Lett 2012;327:123-133.
15. Ivashkevich AN, Martin OA, Smith AJ, Redon CE, Bonner WM, Martin RF, Lobachevsky PN. gammaH2AX foci as a measure of DNA damage: A computational approach to automatic analysis. Mutat Res 2011;711:49-60.
16. Qvarnstrom OF, Simonsson M, Johansson KA, Nyman J, Turesson I. DNA double strand break quantification in skin biopsies. Radiother Oncol 2004;72:311-317.
17. Cai Z, Vallis KA, Reilly RM. Computational analysis of the number, area and density of gamma-H2AX foci in breast cancer cells exposed to (111)In-DTPA-hEGF or gamma-rays using Image-J software. Int J Radiat Biol 2009;85:262-271.
18. Bocker W, Iliakis G. Computational Methods for analysis of foci: Validation for radiation-induced gamma-H2AX foci in human cells. Radiat Res 2006;165:113-124.
19. Barber PR, Locke RJ, Pierce GP, Rothkamm K, Vojnovic B. Gamma-H2AX foci counting: image processing and control software for high-content screening. Proc SPIE 2007.
20. Markova E, Schultz N, Belyaev IY. Kinetics and dose-response of residual 53BP1/gamma-H2AX foci: Co-localization, relationship with DSB repair and clonogenic survival. Int J Radiat Biol 2007;83:319-329.
21. Roch-Lefevre S, Mandina T, Voisin P, Gaetan G, Mesa JE, Valente M, Bonnesoeur P, García O, Voisin P, Roy L. Quantification of gamma-H2AX foci in human lymphocytes: A method for biological dosimetry after ionizing radiation exposure. Radiat Res 2010;174:185-194.
22. Runge R, Hiemann R, Wendisch M, Kasten-Pisula U, Storch K, Zophel K, Fritz C, Roggenbuck D, Wunderlich G, Conrad K, et al. Fully automated interpretation of ionizing radiation-induced gammaH2AX foci by the novel pattern recognition system AKLIDES(R). Int J Radiat Biol 2012;88:439-447.
23. Willitzki A, Hiemann R, Peters V, Sack U, Schierack P, Rodiger S, Anderer U, Conrad K, Bogdanos DP, Reinhold D, et al. New platform technology for comprehensive serological diagnostics of autoimmune diseases. Clin Dev Immunol 2012;2012: 284740.
24. Jucha A, Wegierek-Ciuk A, Koza Z, Lisowska H, Wojcik A, Wojewodzka M, Lankoff A. FociCounter: A freely available PC programme for quantitative and qualitative analysis of gamma-H2AX foci. Mutat Res 2010;696:16-20.
25. Furia L, Pelicci PG, Faretta M. A computational platform for robotized fluorescence microscopy (II): DNA damage, replication, checkpoint activation, and cell cycle progression by high-content high-resolution multiparameter image-cytometry. Cytometry A 2013;83:344-355.
26. Kim S, Jun DH, Kim HJ, Jeong KC, Lee CH. Development of a high-content screening method for chemicals modulating DNA damage response. J Biomol Screen 2011; 16:259-265.
27. Valente M, Voisin P, Laloi P. Automated gamma-H2AX focus scoring method for human lymphocytes after ionizing radiation exposure. Radiat Meas 2011;46:871-876.
28. Turner HC, Brenner DJ, Chen Y, Bertucci A, Zhang J, Wang H, Lyulko OV, Xu Y, Shuryak I, Schaefer J, et al. Adapting the gamma-H2AX assay for automated processing in human lymphocytes. I. Technological aspects. Radiat Res 2011;175:282-290.
29. Garty G, Chen Y, Salerno A, Turner H, Zhang J, Lyulko O, Bertucci A, Xu Y, Wang H, Simaan N, et al. The RABIT: A rapid automated biodosimetry tool for radiological triage. Health Phys 2010;98:209-217.
30. Garty G, Chen Y, Turner HC, Zhang J, Lyulko OV, Bertucci A, Xu Y, Wang H, Simaan N, Randers-Pehrson G, et al. The RABiT: A rapid automated biodosimetry tool for

radiological triage. II. Technological developments. Int J Radiat Biol 2011;87:776-790.

31. Hiemann R, Hilger N, Sack U, Weigert M. Objective quality evaluation of fluorescence images to optimize automatic image acquisition. Cytometry A 2006;69:182-184.
32. Hiemann R, Hilger N, Michel J, Nitschke J, Bohm A, Anderer U, Weigert M, Sack U. Automatic analysis of immunofluorescence patterns of HEp-2 cells. Ann NY Acad Sci 2007;1109:358-371.
33. Hiemann R, Buttner T, Krieger T, Roggenbuck D, Sack U, Conrad K. Challenges of automated screening and differentiation of non-organ specific autoantibodies on HEp-2 cells. Autoimmun Rev 2009;9:17-22.
34. Bonner WM, Redon CE, Dickey JS, Nakamura AJ, Sedelnikova OA, Solier S, Pommier Y. GammaH2AX and cancer. Nat Rev Cancer 2008;8:957-967.
35. Herman-Edelstein M, Rozen-Zvi B, Zingerman B, Lichtenberg S, Malachi T, Gafter U, Ori Y. Effect of immunosuppressive drugs on DNA repair in human peripheral blood mononuclear cells. Biomed Pharmacother 2012;66: 111-115.
36. Ori Y, Herman-Edelstein M, Zingerman B, Rozen-Zvi B, Gafter U, Malachi T, Gafter-Gvili A. Effect of immunosuppressive drugs on spontaneous DNA repair in human peripheral blood mononuclear cells. Biomed Pharmacother 2012;66: 409-413.
37. O'Driscoll M, Jeggo PA. CsA can induce DNA double-strand breaks: Implications for BMT regimens particularly for individuals with defective DNA repair. Bone Marrow Transplant 2008;41:983-989.
38. Dickey JS, Redon CE, Nakamura AJ, Baird BJ, Sedelnikova OA, Bonner WM. H2AX: Functional roles and potential applications. Chromosoma 2009;118:683-692.
39. Davies C. Introduction to immunoassay principles. In: Wild DG, editor. The Immunoassay Handbook. Oxford: Elsevier Ltd; 2005. pp 3-37.
40. Mader RM, Steger GG, Moser K, Rainer H, Krenmayr P, Dittrich C. Instability of the anticancer agent etoposide under in vitro culture conditions. Cancer Chemother Pharmacol 1991;27:354-360.
41. Redon CE, Dickey JS, Bonner WM, Sedelnikova OA. gamma-H2AX as a biomarker of DNA damage induced by ionizing radiation in human peripheral blood lymphocytes and artificial skin. Adv Space Res 2009;43:1171-1178.
42. Thoms KM, Kuschal C, Oetjen E, Mori T, Kobayashi N, Laspe P, Boeckmann L, Schön MP, Emmert S. Cyclosporin A, but not everolimus, inhibits DNA repair mediated by calcineurin: Implications for tumorigenesis under immunosuppression. Exp Dermatol 2011;20:232-236.
43. Guo F, Li J, Du W, Zhang S, O'Connor M, Thomas G, Kozma S, Zingarelli B, Pang Q, Zheng Y. mTOR regulates DNA damage response through NF-kappaB-mediated FANCD2 pathway in hematopoietic cells. Leukemia 2013. Mar 29. doi: 10.1038/leu.2013.93. [Epub ahead of print].
44. Bandhakavi S, Kim YM, Ro SH, Xie H, Onsongo G, Jun CB, Kim DH, Griffin TJ. Quantitative nuclear proteomics identifies mTOR regulation of DNA damage response. Mol Cell Proteomics 2010;9:403-414.